Chemosphere 241 (2020) 125025

Contents lists available at ScienceDirect

Chemosphere

journal homepage: www.elsevier.com/locate/chemosphere

Formation of metal-organic ligand complexes affects solubility of metals in airborne particles at an urban site in the Po valley

Andrea Tapparo [a], Valerio Di Marco [a], Denis Badocco [a], Sara D'Aronco [a], Lidia Soldà [a], Paolo Pastore [a], Brendan M. Mahon [b], Markus Kalberer [b, c], Chiara Giorio [a, b, *]

[a] Department of Chemical Sciences, University of Padua, via Marzolo 1, 35131, Padova, Italy
[b] Department of Chemistry, University of Cambridge, Lensfield Road, Cambridge, CB2 1EW, United Kingdom
[c] Department of Environmental Sciences, University of Basel, Klingelbergstrasse 27, 4056, Basel, Switzerland

HIGHLIGHTS

- Solubility and speciation of metal ions released by PM in aqueous solutions simulating fog and rainwater was investigated.
- Solubility of Al, Cr, and Fe was strongly correlated to the concentrations of oxalate.
- Succinate and malonate moderately affected the solubility of Cr.
- Cu, Zn, Mn, Pb, and Ni were partly complexed by organic acids in solution.
- Direct detection of an iron-oxalate complex was also performed in aerosol sample extracts.

ARTICLE INFO

Article history:
Received 14 July 2019
Received in revised form
28 September 2019
Accepted 30 September 2019
Available online 1 October 2019

Handling Editor: R Ebinghaus

Keywords:
Metal-ligand complexes
Deliquescent aerosol
Urban $PM_{2.5}$
Oxalate
Iron

ABSTRACT

Metals in atmospheric aerosols play potentially an important role in human health and ocean primary productivity. However, the lack of knowledge about solubility and speciation of metal ions in the particles or after solubilisation in aqueous media (sea or surface waters, cloud or rain droplets, biological fluids) limits our understanding of the underlying physico-chemical processes. In this work, a wide range of metals, their soluble fractions, and inorganic/organic compounds contained in urban particulate matter (PM) from Padua (Italy) were determined. Metal solubility tests have been performed by dissolving the PM in water and in solutions simulating rain droplet composition. The water-soluble fractions of the metal ions and of the organic compounds having ligand properties have been subjected to a multivariate statistical procedure, in order to elucidate associations among the aqueous concentrations of these PM components in simulated rain droplets. In parallel, a multi-dimensional speciation calculation has been performed to identify the stoichiometry and the amount of metal-ligand complexes theoretically expected in aqueous solutions. Both approaches showed that the solubility and the aqueous speciation of metal ions were differently affected by the presence of inorganic and organic ligands in the PM. The solubility of Al, Cr, and Fe was strongly correlated to the concentrations of oxalic acid, as their oxalate complexes represented the expected dominant species in aqueous solutions. Oxalates of Al represented ~98% of soluble Al, while oxalates of Cu represented 34–75% of the soluble Cu, and oxalates of Fe represented 76% of soluble Fe. The oxidation state of Fe can strongly impact the speciation picture. If Fe is present as Fe(II) rather than Fe(III), the amount of Cr and Cu complexed with diacids can increase from 75% to 94%, and from 32% to 53%, respectively. For other metals, the solubility depended on the formation of soluble aquo-complexes, hence with a scarce effect of the organic ligands. An iron-oxalate complex was also directly detected in aerosol sample extracts.

© 2019 The Authors. Published by Elsevier Ltd. This is an open access article under the CC BY license (http://creativecommons.org/licenses/by/4.0/).

1. Introduction

Despite air quality policies established worldwide, the progress in reducing airborne particulate matter (PM) has been slow in

* Corresponding author. Department of Chemical Sciences, University of Padua, via Marzolo 1, 35131, Padova, Italy.
E-mail address: chiara.giorio@unipd.it (C. Giorio).

https://doi.org/10.1016/j.chemosphere.2019.125025
0045-6535/© 2019 The Authors. Published by Elsevier Ltd. This is an open access article under the CC BY license (http://creativecommons.org/licenses/by/4.0/).

recent years and PM still remains one of the major polluting agents in the urban atmosphere, posing a substantial burden for public health (Harrison et al., 2010; Lelieveld et al., 2019; Raaschou-Nielsen et al., 2013; Shiraiwa et al., 2017). According to WHO about 90% of the world's population live in areas with unhealthy air, leading to increased mortality and morbidity (WHO, 2016). Air pollution contributes to total mortality more than malaria and HIV combined on a global scale (Lelieveld et al., 2015) and represents the largest environmental risk factor behind premature deaths (Burnett et al., 2018).

The majority of epidemiological studies have used particulate mass (PM_{10} or $PM_{2.5}$) as the metric of choice, largely because of the availability of monitoring data. However, this approach is considered incomplete and can lead to an underestimation of PM risk (Harrison et al., 2010). Despite toxicological studies have shown that chemical composition may play an important role in $PM_{2.5}$ -induced toxicity (Perrone et al., 2010), the chemical species responsible for PM toxicological properties remain a subject of investigation (Decesari et al., 2017). The adverse health effects of $PM_{2.5}$ can be ascribed to polycyclic aromatic hydrocarbons (PAHs) and their nitrated or oxygenated (e.g. quinones) derivatives (Giorio et al., 2019a), the primary biogenic fraction, such as pathogenic bacteria and bacterial endotoxins (Franzetti et al., 2011; Topinka et al., 2011), and water soluble PM fractions such as water soluble organic (WSOC) and inorganic compounds, and metal ions like Zn, Pb and Ni (Birmili et al., 2006; Chen and Lippmann, 2009; Oberdörster et al., 2005; Zhang et al., 2015). The toxic effects caused by Al, Fe and Cu can be also important, as these ions represent the major metal components in PM arising from different sources (Deguillaume et al., 2005).

The bioavailability, rather that the total concentration, of pollutants released by PM in water, as it occurs on the lung surface after inhalation, is expected to correlate with the observed toxic effects. In turn, the bioavailability of each compound strongly depends on its chemical speciation, i.e. on the chemical form by which it is dissolved in solution. As many WSOC and inorganic compounds have coordinating properties towards metal ions, bioavailability depends on the stoichiometry and stability constants of the complexes formed in solution between the metal ions and the ligands contained in PM, after PM enters into contact with water (Giorio et al., 2017; Scheinhardt et al., 2013; Wei et al., 2019). Therefore, a more complete risk assessment of PM requires not only the knowledge of the total concentration of all compounds contained in PM, but also of the stoichiometry of the metal-ligand complexes formed, and of their concentration. This "speciation" approach has been introduced in a fundamental review by Okochi and Brimblecombe (2002). However, detailed investigations on this topic are scarce. The majority of the studies relate the speciation of the PM metal ions with ligands already present in the environment (marine environment or surface waters), whereas only very few studies consider ligands present in the aerosol particles themselves (DePalma et al., 2011; Elzinga et al., 2011; Jickells et al., 2005; Paris et al., 2011; Paris and Desboeufs, 2013; Schroth et al., 2009; Wang et al., 2007). A study from Scheinhardt et al. (2013) suggested that metal-ligand interactions may be an important phenomenon in deliquescent aerosol in the urban atmosphere. As the particles travel deeper into the respiratory system, consisting of wet walled respiratory tracts, they encounter increasing humidity: ~40% in the mouth, ~60% in the pharynx, to finally approaching near water saturation ~99.5% in the deep airways. Hygroscopic particles moving from a region of low ambient humidity into one of high humidity would be expected to increase in size due to water uptake and this will favour coordination chemistry (Tong et al., 2014).

The northern Italian Po Valley, a semi-closed basin surrounded by complex orography, represents a natural laboratory for studying aqueous phase processing of aerosol. It is one of the major European air pollution hotspots and environmental conditions favour fog events during the winter. In this work, an urban PM (Padua, Italy) was subjected to a chemical characterisation in order to identify and quantify the most relevant metal ions and inorganic/organic compounds. Metal content has been determined by inductively coupled plasma mass spectrometry (ICP-MS), whereas organic/inorganic ligands have been measured by ion chromatography (IC). Metal solubility tests have been performed by dissolving the PM in water and in solutions simulating fog/rain composition. The water-soluble fractions of the metal ions and of the inorganic/organic compounds having ligand properties have been subjected to a multivariate statistical procedure. In parallel, a multidimensional speciation calculation has been performed to evaluate the stoichiometry and the concentrations of metal-ligand complexes expected in aqueous solutions. For those complexes expected at higher concentrations their detection was also attempted by nano electrospray ionisation high-resolution mass spectrometry (nanoESI-HRMS) investigations.

2. Experimental

2.1. Chemicals and standard solutions

All reagents were of analytical grade and were used as purchased: 69% HNO_3 (PROLABO, Milan, Italy), multi-element standard solution IV-ICPMS-71A (10 mg L^{-1}) ICP-MS calibration standard (Inorganic Ventures, Christiansburg, VA 24073 USA). All solutions were prepared in ultrapure water obtained with a Millipore Plus System (Milan, Italy, resistivity 18.2 Ω cm^{-1}).

Primary standards for IC analysis were of analytical grade and purchased from Sigma-Aldrich®. Methanol (Optima™ LC/MS, Fisher Chemical) was used for washing and sample extraction for nanoESI-HRMS analysis.

2.2. Aerosol sampling

Teflon filters (PALL, fiberfilm, Ø 47 mm) were pre-washed with large amounts (~250 mL for all filters used) of ultrapure water for three times under ultrasonic agitation for 15 min, changing water each time. Quartz fibre filters (Millipore, AQFA, Ø 47 mm) were decontaminated by baking them at 600 °C for 24 h.

$PM_{2.5}$ samples were collected (sampling time 24 h, from 00.00 to 24.00) at the sampling site located at the 6th floor of the Department of Chemical Sciences of the University of Padova (Italy), using a Zambelli Explorer Plus PM sampler, fitted with a $PM_{2.5}$ certified selector (CEN standard method UNI-EN 14907), and working at a constant flow rate of 2.3 m^3 h^{-1} (Giorio et al., 2013) from the 5th December 2013 to the 1st April 2014, alternating Teflon and quartz filters (see Table S1 in the supplementary material for details).

Weighing of the filters was done for Teflon filters only, before and after sampling, after conditioning at a temperature of 20 ± 1 °C and relative humidity of 50 ± 5% for at least 48 h, as in previous studies (Giorio et al., 2013, 2019b). Filter samples were then stored at −20 °C until analysis.

2.3. Sample preparation

Teflon filters were manually cut into three parts (two parts of ¼ and one part of ½) by a stainless-steel cutter. The use of a stainless-steel cutter did not cause contaminations for the metal determination, as checked by analysis of procedural blanks. For each sample, ¼ filter was treated with 2 mL of 69% nitric acid using a CEM Discover SP-D (CEM Corp., Matthews, NC, USA) microwave

digester at 400 psi and 300 W, with a temperature ramp from 20 °C to 200 °C in 4 min, and maintained at the final conditions for 2 min. The solution was diluted to 3.45% (w/w) nitric acid before analysis by ICP-MS. Another ¼ filter was extracted in 5 mL of a pH 4.5 water solution of H_2SO_4 at 20 °C, simulating fog/rainwater (Beiderwieden et al., 2005; Nieberding et al., 2018; Rodhe et al., 2002; Walna, 2015; Wang et al., 2012), for 24 h without stirring. After that, 4 mL of solution were taken and concentrated HNO_3 (69%) was added to obtain a concentration of 3.45% (w/w) HNO_3 for ICP-MS analysis. Another ½ filter was extracted in 5 mL of ultrapure water at 20 °C for 24 h without stirring. After that, 2 mL were taken and filtered with 0.45 μm syringe filters (Millex®-HV, PVDF, Ø 4 mm) before IC analysis. The other 3 mL were taken, and concentrated HNO_3 was added to obtain a concentration of 3.45% (w/w) HNO_3 for ICP-MS analysis.

Quartz fibre filters were extracted according to the procedure already described elsewhere (Kourtchev et al., 2014) before analysis with nanoESI-HRMS. For each filter sample, the outer ring of the filter, which had been in contact with the filter holder during sample collection, was removed to prevent contamination and a portion of the filter (the whole filter in the case of blanks and ¼ in all other cases) was cut into small (*ca.* 25–100 mm^2) pieces and placed in a glass vial. The pieces of quartz filter were then covered with 5 mL of methanol and extracted by ultrasonic agitation for 30 min in slurry ice. The resulting methanol extracts were then transferred to a new pre-cleaned vial and concentrated via evaporation under a gentle stream of nitrogen (BOC, Guildford, UK) to *ca*. 2 mL on a hotplate (SD160, Stuart, Stone, UK), which was kept at 35 °C. The concentrated extracts were filtered through two syringe PTFE filters (ISO-Disc™, Supelco, with pore sizes of 0.45 μm and 0.22 μm). The filtered extracts were then concentrated further, by evaporation under a gentle stream of nitrogen, to *ca.* 0.1 mL and kept in a washed glass vial at −20° in darkness until analysis.

For each analysis type, procedural blanks (unexposed filters) were also obtained and analysed.

2.4. Instrumental analysis

2.4.1. Analysis of metals with ICP-MS

All elements were determined by using an ICP-MS (Agilent 7700x, Agilent Technologies, Santa Clara, CA, USA). The operating conditions and data acquisition parameters are reported in previous studies (Badocco et al., 2014; Giorio et al., 2019b). The ICP-MS was tuned daily using a 1 μg L^{-1} tuning solution containing ^{140}Ce, ^{59}Co, ^{7}Li, ^{205}Tl and ^{89}Y (Agilent Technologies, UK). The ratio 156/140 representing CeO/Ce is tuned to approximately 1% or less. The ratio 70/140 representing Ce^{2+}/Ce is maintained below 3%. A 50 μg L^{-1} solution of ^{45}Sc and ^{115}In (Aristar®, BDH, UK) prepared in 3.45% (w/w) nitric acid was used as an internal standard through addition to the sample solution via a T-junction.

Multielement standard solutions were prepared in 3.45% (w/w) HNO_3. The calibration solutions were prepared by gravimetric serial dilution from multi-element standard solutions in the range between 1 ng L^{-1} and 1 mg L^{-1}. The detection limit of each element was determined using five concentration levels replicated nine times. Blank samples of ultrapure water and reagents were also prepared using the same procedures adopted for the samples.

2.4.2. Analysis of soluble inorganic anions and short-chain organic acids

Instrumental analysis was performed by injecting 20 μL of water extracts in a Dionex IC system equipped with an a GP50 Gradient Pump, an EG40 eluent generation system fitted with a Dionex EGC III KOH RFIC™ eluent generator cartridge, a LC25 oven, and an ED40 Electrochemical Detector (in conductometric detection mode), and fitted with a Dionex IonPac AG11-HC (2 × 50 mm) guard column, a Dionex IonPac AS11-HC (2 × 250 mm) chromatographic column, and a Dionex AERS 500 (2 mm) self-regenerating suppressor (suppression current 100 mA). Chromatographic separation was achieved at room temperature (~20 °C), with a flow rate of 300 μL/min, and elution gradient: 0–3 min 3 mM KOH, 3–5 min linear gradient from 3 mM to 10 mM KOH, 5–12 min linear gradient from 10 mM to 20 mM KOH, 12–20 min 20 mM KOH, 20–24 min linear gradient from 20 mM to 40 mM KOH and 24–35 min 40 mM KOH. Equilibration time at the beginning of each chromatographic run was 7 min.

External calibration was performed daily with standard solutions in the range 0.1–50 mg L^{-1} of each analyte in ultrapure water prepared from suitable primary standards purchased from Sigma-Aldrich®.

2.4.3. nanoESI-HRMS analysis

Samples were analysed using a high-resolution LTQ-Orbitrap mass spectrometer (Thermo Scientific™, Bremen, Germany), with a mass resolving power of 100,000 at *m/z* 400 and a typical mass accuracy within ±2 ppm, equipped with a chip-based nanoESI source (Triversa NanoMate Advion, Ithaca, NY, USA) operating in both positive and negative ionisation mode.

Samples were sprayed at a gas (N_2) pressure of 0.90 psi, ionisation voltage of −1.4 kV in negative ionisation mode and gas pressure of 0.30 psi, ionisation voltage of 1.8 kV in positive ionisation mode, and with a transfer capillary temperature of 210 °C as used in previous studies (Giorio et al., 2015, 2019a; Kourtchev et al., 2014).

For each sample, data were acquired in full scan in the *m/z* ranges 100–650 and 150–900 for 1 min each in both positive and negative ionisation modes. The mass spectrometer was calibrated routinely using a Pierce LTQ Velos ESI Positive Ion Calibration Solution and a Pierce ESI Negative Ion Calibration Solution (Thermo Fisher).

The averaged spectra for each sample and each scan range were then exported as a binary list of *m/z* values and peak intensities using the proprietary software Xcalibur™ 2.1 (Thermo Scientific™, Bremen, Germany). Exported data were processed using a code written *in-house* to isolate signals attributable to metal-ligand complexes of interest based on their exact mass and isotopic pattern and taking into account also the possibility to form adducts with the most common anions and cations present as impurities in the solvents.

2.5. Statistical analysis

Limits of detection (LODs) of both IC and ICP-MS measurements were evaluated using a two-component variance regression using the ordinary least squares (OLS) regression as detailed in previous studies (Badocco et al., 2015a, 2015b).

Data have been statistically analysed through F-test, Tukey's test, analysis of variance (ANOVA), and principal component analysis (PCA) using the software Statistica 7 (StatSoft Inc., Tulsa, OK). A 95% significance level was considered for all statistical tests.

2.6. Speciation calculations

The concentration of each metal-ligand complex was calculated at the given pH value by means of the software PITMAP (Di Marco, 1998). Briefly, mass balance equations are solved, i.e. species concentration at equilibrium are obtained, by means of the Newton–Raphson method (Press et al., 2007). The metal ions and ligands, and their concentrations were chosen on the basis of the analytical results obtained in the previous sections. The input

thermodynamic data (stoichiometry and stability constant of the complexes, including metal-aquo-complexes) have been obtained from the literature (ScQuery v.5.84, 2005). All metal ions and ligands were considered to be simultaneously present in solution, in order to obtain a speciation picture which includes all competitive components in solution.

3. Results and discussion

3.1. $PM_{2.5}$ composition

Atmospheric conditions during the sampling campaign were characterised by low temperatures, close to 0 °C during the first part of the campaign and reaching a maximum temperature of 14 °C toward the end of the campaign, high relative humidity (RH), often above 90%, and high aerosol loading with $PM_{2.5}$ concentrations ranging between 12 and 113 μg m^{-3} (Fig. 1, Tables S1 and S2). Such conditions favour aqueous phase processing of aerosol particles and fog events which create a suitable environment for coordination chemistry to occur. $PM_{2.5}$ concentrations were in the range of those observed in other northern Italian cities, such as Bologna in which average $PM_{2.5}$ values were in the range 31–59 μg m^{-3} in the years 2011–2013 (Pietrogrande et al., 2014), and Milan in which average $PM_{2.5}$ concentrations in the winter were 60 μg m^{-3} in the years 2006–2009 (Perrone et al., 2012). The results of the ion chromatography analysis (Fig. 1, Table 1 and Table S3) show that nitrate and sulfate are the main contributing species in our samples, as expected (Giorio et al., 2013, 2017).

3.1.1. Organic acids

Short-chain dicarboxylic acids, i.e. oxalate, succinate, and malonate, represent abundant components in our samples. These compounds have the ability to act as ligands for metal ions present in $PM_{2.5}$ and therefore could affect their solubility. They can be produced by atmospheric oxidation of a wide range of volatile and non-volatile organic compounds of both natural and anthropic origin through gas and condensed phase reactivity (Kawamura and Bikkina, 2016; Sareen et al., 2016). As expected for a continental aerosol, oxalate is the diacid present with the highest concentration in our samples. The median concentrations of dicarboxylic acids (Table 1) in this sampling campaign were 217 ng m^{-3} for oxalate, 19 ng m^{-3} for malonate, and 57 ng m^{-3} for succinate. These values are in line with those found in Bologna, Italy, another city in the Po Valley, in which average concentrations of malonate were in the range 21.7–29.7 ng m^{-3} and concentrations of succinate were in the range 26.8–112.1 ng m^{-3} in the years 2011–2013 (Pietrogrande et al., 2014). The concentration levels were not far also from those found in Hong Kong in the years 2000, where average values were around 360 ng m^{-3}, 20 ng m^{-3}, and 60 ng m^{-3} for oxalate, malonate and succinate, respectively (Yao et al., 2004), and 2003 when concentration values ranged between 179–2372 ng m^{-3}, 38–324 ng m^{-3}, and 35–297 ng m^{-3} for oxalate, malonate and succinate, respectively (Li and Yu, 2005).

The ratio of malonic to succinic acid <1 for the majority of the campaign indicates a rather freshly emitted organic aerosol from vehicular traffic rather than photochemically aged (Yao et al., 2004). Succinate may be formed also by oxidation of unsaturated fatty acids emitted with sea spray (Kerminen et al., 2000) and the presence of methanesulfonic acid (MSA) in our samples suggests

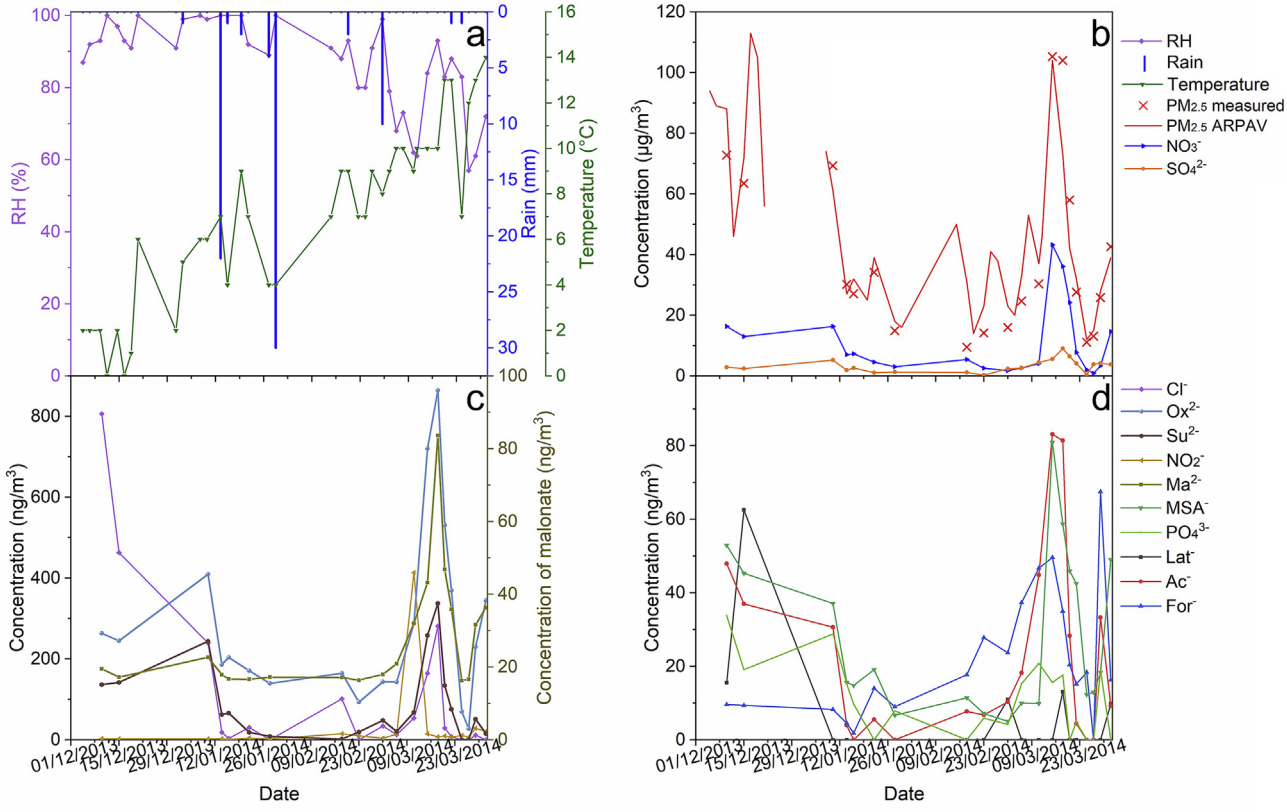

Fig. 1. Meteorological conditions (a), $PM_{2.5}$ concentrations (from both the present study and the Regional Environmental Agency, ARPAV), nitrate and sulfate concentrations (b), dicarboxylic acids and nitrite concentrations (c), and other anion concentrations (d) in $PM_{2.5}$ during the sampling campaign from the 5th December 2013 to the 1st April 2014. Lat^- = lactate, Ac^- = acetate, For^- = formate, MSA^- = methanesulfonate, Su^{2-} = succinate, Ma^{2-} = malonate, Ox^{2-} = oxalate.

Table 1
Median, maximum, 75th percentile, 25th percentile and minimum concentrations (ng m^{-3}) of the inorganic and organic anions (ordered according to their retention times) determined in $PM_{2.5}$ in the winter campaign (5th December 2013 to 1st April 2014, N = 20). Lat^- = lactate, Ac^- = acetate, For^- = formate, MSA^- = methanesulfonate, Su^{2-} = succinate, Ma^{2-} = malonate, Ox^{2-} = oxalate. Measurement uncertainties are between 2 and 4%.

	Lat^-	Ac^-	For^-	MSA^-	Cl^-	NO_2^-	NO_3^-	Su^{2-}	Ma^{2-}	SO_4^{2-}	Ox^{2-}	PO_4^{3-}
Median	<LOD	9.8	17.0	17.0	23.9	7.2	6232.1	57.0	18.8	2765.9	216.9	8.8
Max	62.5	83.1	67.5	80.9	806.2	413.3	43207.3	337.7	83.6	9034.5	864.2	33.8
75th perc.	2.5	34.2	29.6	45.5	117.2	14.2	15007.0	135.1	33.0	4258.7	350.7	17.9
25th perc.	<LOD	4.3	9.3	11.1	2.8	3.01	2926.4	17.8	17.0	1727.3	143.3	<LOD
Min	<LOD	<LOD	<LOD	5.0	<LOD	<LOD	878.1	<LOD	16.3	258.7	27.7	<LOD

that atmospheric transport is taking marine biogenic emissions to our inland urban location (Yao et al., 2004). Therefore, a marine contribution to succinate cannot be ruled out and the organic aerosol may be more photochemically aged than predicted from the malonic to succinic acid ratio. A median ratio of acetic to formic acid of about 0.5 indicates a secondary origin of carboxylic acids rather than from primary emissions (Grosjean, 1992; Mkoma et al., 2012).

Concerning monocarboxylic acids, median concentrations in our samples were 9.8 and 17.0 ng m^{-3} for acetate and formate, respectively, higher than 5.4 and 0.71 ng m^{-3} found in Morogoro, Tanzania (Mkoma et al., 2012). Formate concentrations were lower than those found in the US in Los Angeles (49 ng m^{-3}) and Atlanta (39 ng m^{-3}) in the summer of 2010 (Liu et al., 2012). Both formate and acetate concentrations were lower than those found in urban and rural $PM_{2.5}$ in Spring 2007 in Londrina, Brazil (Freitas et al., 2012).

3.1.2. Metals

Table 2 shows the total concentration of each metal (M_T) determined in $PM_{2.5}$, as median of 20 samples, together with the median soluble fractions in water (M_H) and in water at a pH of 4.5 (M_A) simulating fog/rainwater. Data for each individual sample are reported in Tables S4–S9. The elements present at the highest concentrations in our samples are K, Fe, Zn, Mg, Ca and Al. The soluble fractions, however, do not follow the same trend likely because the solubilisation is influenced by their speciation in the PM matrix itself, e.g. compound of origin and oxidation state of the metal, and in solution. In general, the soluble fraction is larger at pH 4.5, simulating a fog or rainwater, rather than at autogenic pH (measured pH ranged between 4.5 and 5.6, median value 5.0). Autogenic pH for some samples was close to, or equal to, a value of 4.5 and therefore the soluble fractions M_H and M_A were the same within uncertainty.

Concerning the total amounts of metals in $PM_{2.5}$, the values found in the present study were around the same order of magnitude as in other urban locations in Europe. For example, Fe median concentration was 240 ng m^{-3} in this series of samples, which is slightly higher than 71.5–206.3 ng m^{-3} found at five sites in the Netherlands (Mooibroek et al., 2011), within the range 54–457 ng m^{-3} found in three sites in Poland (Rogula-Kozłowska et al., 2014), and within the range 0.09–1152 ng m^{-3} found in rural background sites across Europe (Fomba et al., 2015). Cu median concentration was 11 ng m^{-3} in this study, within the range 5–81 ng m^{-3} found across urban sites in Spain (Querol et al., 2008), slightly above the range 2.5–10.9 ng m^{-3} found at five sites in the Netherlands (Mooibroek et al., 2011), higher than the 2.8 ng m^{-3} in an urban site in Birmingham (UK) (Pant et al., 2017) and 0.08 ng m^{-3} in Naples (Italy) (Chianese et al., 2019), within the range 0.10–58 ng m^{-3} found in rural background sites across Europe (Fomba et al., 2015). Zn median concentration was 48 ng m^{-3} in this study, not far from the concentrations 14–420 ng m^{-3} found across Spain (Querol et al., 2008), 90.5–99.5 ng m^{-3} at five sites in the Netherlands (Mooibroek et al., 2011), 14.1 ng m^{-3} in an urban site in Birmingham (Pant et al., 2017), 41.3–42.4 ng m^{-3} in Naples (Chianese et al., 2019) and 1.1–79.5 ng m^{-3} in rural background sites across Europe (Fomba et al., 2015). Ba and Cr median concentrations were 16 and 2.2 ng m^{-3}, respectively in this study. These values are within the range 12–41 and 2–25 ng m^{-3} found across urban sites in Spain (Querol et al., 2008) for Ba and Cr, respectively, and 4.5–11 and 2.7–3.7 ng m^{-3} found at five sites in the Netherlands (Mooibroek et al., 2011) for Ba and Cr, respectively. Al median concentration of 82 ng m^{-3} of this study is within the range 31–457 ng m^{-3} found in three sites in Poland (Rogula-Kozłowska et al., 2014). Pb, As and Cd median concentrations of 12, 1.2 and 0.55 ng m^{-3}, respectively, found in this study are close to the concentrations reported in the review by Csavina et al. (2012) for sites affected by smelting and mining operations.

Table 2
Limits of detection (LODs), median concentrations (total amount, M_T), percentage of solubilisation at autogenic pH (M_H) and at an acidic pH of 4.5 (M_A) of the elements present in $PM_{2.5}$ samples collected from the 5th December 2013 to the 1st April 2014. Measurement uncertainty is <5% (Badocco et al., 2015a).

Element	LOD (ng m^{-3})	M_T (ng m^{-3})	M_H (%)	M_A (%)
Ag	0.27	<LOD		
Al	0.10	82	11	14
As	0.0070	1.2	28	40
B	0.35	570	1	1
Ba	0.083	16	0	29
Be	0.23	<LOD		
Ca	0.39	33	52	82
Cd	0.0080	0.55	26	39
Ce	0.011	0.12	4	7
Co	0.0040	0.14	7	9
Cr	0.0060	2.2	13	19
Cs	0.010	<LOD		
Cu	0.0050	11	24	35
Eu	0.0067	<LOD		
Fe	0.27	240	6	11
Ga	0.012	3	0	24
Gd	0.013	<LOD		
K	1.0	404	60	83
La	0.0030	0.06	4	6
Mg	1.1	47	11	54
Mn	0.030	7.4	29	42
Na	0.25	n.d.[a]	n.d.[a]	n.d.[a]
Nd	0.0040	0.027	2	1
Ni	0.16	<LOD		
P	2.8	8.9	33	59
Pb	0.0060	12	6	12
Pr	0.0010	<LOD		
Rb	0.0070	0.94	53	76
Se	0.056	0.33	41	56
Sm	0.0040	0.004	8	17
Sr	0.0030	0.58	34	55
Th	0.0075	<LOD		
Tl	0.0030	0.031	49	65
U	0.013	<LOD		
V	0.011	1.03	41	61
Zn	0.011	48	79	78

[a] n.d. = not determined, due to contaminations of blank filters.

3.2. Correlations between metals and organic ligands

In order to investigate the influence of the presence of organic ligands on the solubilisation of the elements a Pearson correlation test was used. Elements to be considered for this purpose were selected using the ANOVA test. We selected only the elements that had a sample-to-sample variance larger than the variance of the analytical measurement and a concentration value higher than the LOD in at least the 70% of the samples (N = 20). Selected elements for further analysis were: Al, As, B, Ba, Ca, Cd, Ce, Co, Cr, Cu, Fe, Ga, K, La, Mg, Mn, Nd, P, Pb, Rb, Se, Sm, Sr, Tl, V, and Zn. An example of the results of the correlation analysis is reported in Table 3. The soluble fraction of Fe (in percentage) is significantly correlated with organic species that have ligand properties. The significance follows the order oxalate > succinate > malonate. A similar result was obtained for Cu, while Pb is significantly correlated with oxalate. Solubility of Zn does not seem to be influenced by the ligands while phosphate may influence the solubility of Pb but not that of Fe, and Cu. This is further discussed in section 3.3.

Experimental data were additionally subjected to a PCA to look for possible association between the elements and the organic ligands that may facilitate their solubilisation and therefore enhance their bioavailability. For the PCA we considered all organic and inorganic anions listed in Tables 1 and 2, and the elements selected through the ANOVA test excluding Ba, B, La, Ce, Nd, Sm, Tl and U because present at concentrations only slightly above the LOD.

Fig. 2a and b show the loading and score plots referred to the PCA applied to the total concentration of metals. The first two principal components (PCs) explain ~60% of the variance. The loading plot (Fig. 2a) shows that the elements can be divided into two groups: the first group correlates with PC1 and all ligands while the second group, made of Ca, Mg, Sr and Zn which are characterised by a high solubility (Table 2), correlates with PC2.

Fig. 2c and d show the loading and score plots referred to the PCA applied to the soluble fractions of the metals at autogenic pH (M_H/M_T) and pH 4.5 (M_A/M_T). The first two principal components (PCs) explain only ~46% of the variance. The additional PCs did not bring any information on correlations between soluble metal ions and organic ligands, so they are not reported in this study.

The loading plot (Fig. 2c) shows that the soluble fraction of Fe, both in water and at pH 4.5, is basically superimposed to oxalate, and the other dicarboxylic acids (succinate and malonate), which is in agreement with a previous study on desert dusts (Paris and Desboeufs, 2013). PC1 indicates that the elements whose solubilisation is most influenced by the presence of the organic ligands are Fe and Pb. Differently, the solubilisation of Cu, Mn and V are explained also by PC2. Very soluble metals such as Zn, K, Rb, Mg are clustered toward the top part of the plane defined by the first two PCs and strongly correlated with PC2. Sr, Ca and Al cluster together toward the bottom-right of the plane defined by the first two PCs. These elements are of crustal origin and may be present either in a rather refractory chemical form (Al) or be readily soluble (Ca, Sr) so that their solubilisation is not much influenced by the organic component, but it may be influenced by other processes (e.g. hydrolysis). Similarly, the soluble fraction of Cr at pH 4.5 seems to be only slightly influenced by the presence of the dicarboxylic acids while its soluble fraction at autogenic pH is close to the axis origin and so it is not explained by the first two PCs.

The score plots (Fig. 2b and d) show that the samples collected on the 15th and 18th March 2014 are those with the highest concentrations of metals, highest soluble fraction and highest concentration of organic ligands. These two days were characterised by high $PM_{2.5}$ concentrations but also high RH (Fig. 1).

Table 3
p-values of the Pearson correlation tests between the soluble fraction of the elements at autogenic (M_H) and acidic (M_A) pH and selected ligands. Su^{2-} = succinate, Ma^{2-} = malonate, Ox^{2-} = oxalate.

	Su^{2-}	Ma^{2-}	Ox^{2-}	PO_4^{3-}
Zn_H	0.66	0.58	0.50	0.47
Zn_A	0.70	0.60	0.54	0.52
Fe_H	$<10^{-4}$	$<10^{-3}$	$<10^{-6}$	0.19
Fe_A	$<10^{-4}$	$<10^{-3}$	$<10^{-5}$	0.26
Cu_H	<0.05	0.01	<0.05	0.68
Cu_A	0.03	0.04	0.01	0.64
Pb_H	<0.05	0.22	<0.01	<0.01
Pb_A	<0.05	0.49	0.05	<0.03

3.3. Speciation in solution

The speciation of an aqueous solution represents the qualitative and quantitative composition of the solution at the given experimental conditions. Speciation depends on temperature, pH, and concentrations of the system components. When temperature and pH are fixed, the speciation of a given metal ion M^{n+} depends on its concentration, on the concentration of all ligands in solution which can bind M^{n+}, on the concentration of all other metal ions in solution which can compete with the ligands of M^{n+}, and also on the concentration of all ligands which do not bind M^{n+} but bind the competitor metal ions. A reliable speciation model for M^{n+} can therefore be obtained only if all the solution components having binding ability are taken into account, and if stability constants of formation of the complexes are known.

A database was built, which includes the components with complexing ability detected in the soluble fractions of the PM (see Tables 1 and 2). The inorganic and organic compounds included in the database are reported in Table 4 (first row). Monocarboxylates (acetate, formate) and methylsulfonate, although detected in the PM soluble fraction (Table 2), were not included in the database due to their low concentration in solution and especially because they are very weak complexing agents for all metal ions. Therefore, their effect on metal ion speciation can be considered negligible. Other potentially very important ligands present in the aerosol, however not determined in this study, are humic-like and fulvic-like substances. These polyfunctional macromolecules are powerful chelating agents (Borgatta and Navea, 2015; Willey et al., 2000; Win et al., 2018) but, at present, their molecular characterisation, consequent information on the stoichiometry of the complexes and their stability constants is far from complete. These substances, together with microbial proteins, may also be present as siderophores in atmospheric aqueous phases and may affect metal ion solubilisation from aerosol particles (Cheize et al., 2012; Vinatier et al., 2016). The metal ions included in the database are reported in Table 4 (first column). For the speciation calculations, each metal has been considered to be dissolved at only one oxidation state. If more oxidation states would exist for a given metal, the most stable one at environmental conditions was chosen for the speciation calculations. For example, Fe was considered to be dissolved only as Fe^{3+}, Cu only as Cu^{2+}. In the case of Fe, however, additional speciation calculations were performed considering that this metal is only in the oxidation state +2. The chosen oxidation states are explicitly stated in the first column of Table 4. Not all elements detected in the PM soluble fraction (Table 1) have been included in the database. In particular, alkaline metal ions (K^+, Rb^+) have been excluded as they do not display appreciable complexing ability towards ligands in aqueous solutions. Some elements, namely V, As, and Se, are likely present as oxo-compounds in their most stable oxidation states (+5, +5 and + 6, respectively), but only vanadates have appreciable coordinating abilities towards ligands and were included in the database. The acidity constants of the ligands

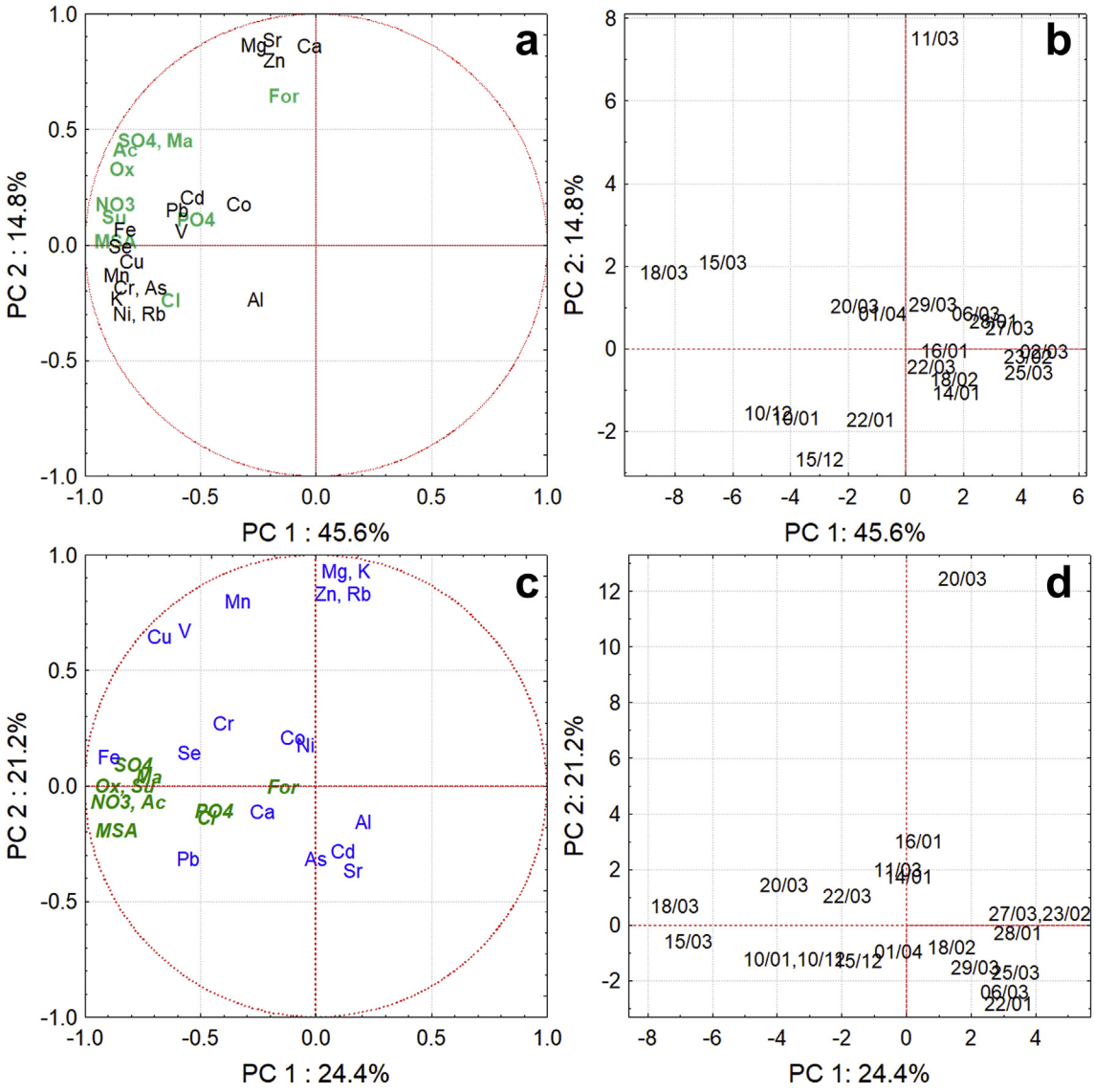

Fig. 2. Loadings (a) and scores (b) of the PCA applied to the total element concentration together with all organic and inorganic anions, and loadings (c) and scores (d) of the PCA applied to the soluble fraction of the elements in water (M_H/M_T) and in water at pH 4.5 (M_A/M_T). For clarity only soluble metals in water at pH 4.5 are reported in panel *c* because the two fractions are always superimposed in the plane defined by the first two PCs with the exception of Cr for which the soluble fraction in water at autogenic pH is not explained by the first two PCs.

(H^+ + ligand), and the stability constants of metal hydroxocomplexes (metal + OH^-) were included, as H^+ and OH^- compete with the metal ions and with the ligands, respectively, in the complex formation.

The IUPAC stability constant database was used as the source of thermodynamic data regarding metal-ligand complex formation (ScQuery v.5.84, 2005). Table 4 reports the stoichiometry and the stability constants of the metal-ligand complexes formed for each metal-ligand pair. Many different speciation models (i.e. formation constants in different aqueous media) were often reported in the literature for each given metal-ligand pair: the model chosen as the most reliable (reported in Table 4) was the one obtained in aqueous solutions at the lowest level of ionic strength, which better resembles atmospheric water phases such as fog and rain waters (Scheinhardt et al., 2013). No mixed complexes (one metal ion + two ligands, or one ligand + two metal ions) were included in the database, with the exceptions of protonated- and hydroxo-ligand complexes.

Speciation calculations have been performed on the basis of the thermodynamic model reported in Table 4, using the metal and ligand concentration data of the sampled PM fractions. The calculation was performed for all sampled solutions considering metal solubility in diluted sulfuric acid solution at pH 4.5, simulating fog and rainwater. Table 5 reports the speciation data obtained for the PM sampled on 10th January 2014. Data are reported as percentage of each metal species relative to the total soluble amount of the same metal. Similar tables were obtained for all other samples, but results do not differ significantly from those reported in Table 5 which can therefore allow us to draw general conclusions.

Table 5 shows two well-defined groups of metal ions. The first group included those elements for which the main (if not only) species in solution was the free metal ion. These elements were the +2 metal cations, i.e. Ca^{2+}, Cd^{2+}, Co^{2+}, Cu^{2+}, Mg^{2+}, Mn^{2+}, Ni^{2+}, Pb^{2+}, Sr^{2+}, and Zn^{2+}, as well as the monocharged VO_2^+. An example of speciation for this kind of metals is reported in Fig. 3a (Zn^{2+}). The only other significant species was the sulfate complex, which

Table 4
Inorganic/organic ligands and metal ions considered for the calculation of the speciation in PM-containing water solutions. Concerning Fe, speciation calculations were performed considering two scenarios in which Fe is present only as Fe^{3+} or only as Fe^{2+}. Ox = oxalate ($C_2O_4^{2-}$), Ma = malonate ($C_3H_2O_4^{2-}$), Su = succinate ($C_4H_4O_4^{2-}$). The most reliable thermodynamic model (stoichiometry and stability constants of the complexes) is reported for every metal-ligand couple as obtained from the Iupac Stability Constant database (ScQuery v.5.84, 2005). Stability constants are given as log(β) and they refer to the general reactions $m\,M + \lambda L + h\,H \rightleftharpoons M_mL_\lambda H_h$. Charges of the complexes are omitted for simplicity.

metal ions	ligands Cl^-	NO_3^-	PO_4^{3-}	SO_4^{2-}	Ox^{2-}	Ma^{2-}	Su^{2-}	OH^-
Al^{3+}	–	–	AlH_2PO_4 19.65 $AlHPO_4$ 17.7 $AlPO_4$ 13.5 $AlPO_4OH$ 8.37 Al_2PO_4 17.42	$AlSO_4$ 3.84 $Al(SO_4)_2$ 5.58	AlHOx 3.84 AlOx 6.97 $Al(Ox)_2$ 12.93 $Al(Ox)_3$ 17.88	AlMa 7.49 $Al(Ma)_2$ 12.62	AlHSu 7.03 AlSu 3.63 AlSuOH −0.53 $AlSu(OH)_2$−5.55	AlOH −5.53 $Al(OH)_2$−11.3 $Al(OH)_3$−17.3 $Al(OH)_4$−23.46
Ca^{2+}	CaCl 0.42	$CaNO_3$ 0.6	$CaHPO_4$ 13.98	$CaSO_4$ 2.19	CaOx 2.08	CaMa 2.50	CaHSu 6.18 CaSu 1.20	–
Cd^{2+}	CdCl 1.98 $CdCl_2$ 2.64 $CdCl_3$ 2.3	$CdNO_3$ 0.40	$CdHPO_4$ 15.19	$CdSO_4$ 2.35	CdOx 2.52 $Cd(Ox)_2$ 4.20	CdMa 2.64	CdSu 2.03	CdOH −9.80 $Cd(OH)_2$−20.19
Co^{2+}	CoCl 0.60 $CoCl_2$ 0.02 $CoCl_3$ −1.71 $CoCl_4$ −4.51	$CoNO_3$ −0.46 $Co(NO_3)_2$−0.30	$CoHPO_4$ 14.56	$CoSO_4$ 2.51	CoOx 3.21 $Co(Ox)_2$ 5.93	CoMa 2.92 $Co(Ma)_2$ 4.60 $Co(Ma)_3$ 5.30	CoSu 2.96	CoOH −8.23 $Co(OH)_2$−17.83
Cr^{3+}	CrCl −1.0	$CrNO_3$ −1.91	$CrPO_4OH$ 8.12 $CrPO_4(OH)_2$−1.92 $CrPO_4(OH)_3$−14.34	$CrSO_4$ 1.6	CrOx 5.34 $Cr(Ox)_2$ 10.51 $Cr(Ox)_3$ 15.44	CrMa 7.06 $Cr(Ma)_2$ 12.85 $Cr(Ma)_3$ 16.15	CrSu 6.42 $Cr(Su)_2$ 10.99 $Cr(Su)_3$ 13.85	CrOH −4.29 $Cr(OH)_2$−9.49 $Cr(OH)_3$−18.00
Cu^{2+}	CuCl 0.83 $CuCl_2$ 0.60	$CuNO_3$ 0.44	$CuHPO_4$ 15.67	$CuSO_4$ 2.27	CuOx 4.60 $Cu(Ox)_2$ 8.70	CuMa 5.13 $Cu(Ma)_2$ 8.81	CuSu 3.02	CuOH −7.95 $Cu(OH)_2$−16.2 $Cu(OH)_3$−26.6
Fe^{2+}	–	–	FeH_2PO_4 22.24 $FeHPO_4$ 15.94	$FeSO_4$ 2.39	FeOx 2.30 $Fe(Ox)_2$ 1.88	FeMa 2.24	FeSu 1.42 $Fe(Su)_2$ 2.92	FeOH −9.63
Fe^{3+}	FeCl 0.67 $FeCl_2$ 1.37	$FeNO_3$ −0.22	FeH_3PO_4 21.48 FeH_2PO_4 23.54 $FeHPO_4$ 22.34 $FeH_5(PO_4)_2$ 45.98 $FeH_4(PO_4)_2$ 46.51 $FeH_3(PO_4)_2$ 43.72 $FeH_7(PO_4)_3$ 69.12 $FeH_6(PO_4)_3$ 68.44	$FeSO_4$ 4.27 $Fe(SO_4)_2$ 6.11	FeOx 7.53 $Fe(Ox)_2$ 13.64 $Fe(Ox)_3$ 18.49	FeMa 7.52 $Fe(Ma)_2$ 13.29 $Fe(Ma)_3$ 16.93	FeSu 7.89 $Fe(Su)_2$ 13.34	FeOH −2.87 $Fe(OH)_2$−6.16 $Fe(OH)_3$−12.16 $Fe(OH)_4$−22.16
Mg^{2+}	MgCl 0.49	$MgNO_3$ 0.06	$MgHPO_4$ 15.04	$MgSO_4$ 2.38	MgOx 2.18	MgMa 2.86	MgSu 1.47	–
Mn^{2+}	MnCl 0.85	$MnNO_3$ −0.15	$MnHPO_4$ 14.79	$MnSO_4$ 2.26	MnOx 3.15 $Mn(Ox)_2$ 4.41	MnMa 3.11	MnSu 2.26	MnOH −10.5
Ni^{2+}	NiCl −0.83 $NiCl_2$ −1.2	$NiNO_3$ −0.22 $Ni(NO_3)_2$−1.0	$NiHPO_4$ 14.54	$NiSO_4$ 2.45	NiOx 3.46 $Ni(Ox)_2$ 6.42	NiMa 3.92 $Ni(Ma)_2$ 6.84	NiSu 3.12	NiOH −8.10 $Ni(OH)_2$−16.87
Pb^{2+}	PbCl 1.50 $PbCl_2$ 2.10 $PbCl_3$ 2.00	$PbNO_3$ 1.15	$PbHPO_4$ 15.64	$PbSO_4$ 2.77	PbOx 3.60 $Pb(Ox)_2$ 6.10	PbMa 3.10	PbSu 2.40	PbOH −7.2 $Pb(OH)_2$−16.1 $Pb(OH)_3$−26.5
Sr^{2+}	SrCl −0.24	$SrNO_3$ 0.7	$SrHPO_4$ 13.72	$SrSO_4$ 1.44	SrOx 1.25 $Sr(Ox)_2$ 1.90	SrMa 1.30	SrSu 0.9	–
VO_2^+	VO_2Cl −0.38	VO_2NO_3 −0.07	$VO_2H_2PO_4$ 20.91 VO_2HPO_4 17.54 $VO_2(HPO_4)_2$ 32.88	VO_2SO_4 0.95	VO_2Ox 6.49 VO_2Ox_2 9.99	–	–	$VO_2(OH)_3$−7.1
Zn^{2+}	ZnCl 0.46	$ZnNO_3$ −0.68	$ZnHPO_4$ 14.86	$ZnSO_4$ 2.03	ZnOx 3.42 $Zn(Ox)_2$ 6.16	ZnMa 2.85	ZnSu 2.47	ZnOH −7.89 $Zn(OH)_2$−14.92
H^+	–	–	HPO_4 12.338 H_2PO_4 19.54 H_3PO_4 21.681	–	HOx 4.266 H_2Ox 5.54	HMa 5.70 H_2Ma 8.53	HSu 5.636 H_2Su 9.84	H_2O 14

represented around 10% of the total metal ion in solution. For Pb^{2+} and in part also for Co^{2+} and Ni^{2+} the sulfate complex was more important, as it represented 25%, 16%, and 14%, respectively, of the total metal ion. For Cu^{2+} the oxalate complex concentration was larger than that of the sulfate complex, and the former represented 21% of total copper in solution. Copper speciation is shown in Fig. 3b. These results indicated that the solubility of the first group of metal ions is scarcely affected by the presence of ligands from the aerosol. Although, the solubility contribution due to SO_4^{2-} contained in PM was generally significant, especially for the toxic Pb^{2+} ion.

The second group of elements included the +3 metal cations, i.e. Al^{3+}, Cr^{3+}, and Fe^{3+}, for which the free metal fraction in solution was low if not negligible. The speciation for Fe^{3+} is reported in Fig. 3c. The main binder for these metal ions was oxalate, in particular for Al and Fe: Al-oxalate complexes represented 99% of total Al in solution, and Fe-oxalate complexes accounted for 76% of total Fe. Only a small fraction of Fe (~1%) was bound to phosphate. Cr displayed a more complicated speciation, as oxalate was a significant but not exclusive binder. 34% of total Cr was complexed by oxalate, but also Cr-succinate (26%) and Cr-malonate complexes (14%) were computed to have significant concentrations in solutions. These results indicated that Al, Cr and Fe solubility from aerosol was mainly, if not exclusively, determined by the ligands contained in the PM among which oxalate was by far the most important. Al and Fe complexes were around 100 times more concentrated than the free metal ions. Therefore, Al and Fe would have dissolved less (~2 orders of magnitude less) in the absence of organic aerosol components. Cr complexes were ca. four times more concentrated than free Cr, so the organic aerosol components

Table 5
Percentages of the various metal ions species calculated on the basis of the thermodynamic model of Table 4, under the hypothesis that Fe was present as Fe(III), for the PM sampled on 10th January 2014 (concentrations in the extraction solution at pH 4.5, simulating rain droplet composition). Only species having percentages above 1% are reported. Free metal ion percentages (given as sum of percentages of M^{n+} and of its hydroxo derivatives) are reported also if below 1%.

metal ion	major species	other important species (>5%)	minor species (<5%)
Al^{3+}	$Al(Ox)_2$ 54%	$Al(Ox)_3$ 37% AlOx 8%	AlMa 1% free Al < 1%
Ca^{2+}	free Ca 91%	$CaSO_4$ 8%	$CaNO_3$ 1%
Cd^{2+}	free Cd 86%	$CdSO_4$ 12%	CdCl 1% $CdNO_3$ 1%
Co^{2+}	free Co 83%	$CoSO_4$ 16%	CoOx 1%
Cr^{3+}	CrSu 25% free Cr 25%	CrMa 13% $CrOx_2$ 13% CrOx 12% $CrOx_3$ 9%	$CrSu_2$ 1% $CrMa_2$ 1%
Cu^{2+}	free Cu 68%	CuOx 21% $CuSO_4$ 8%	$CuOx_2$ 2% CuMa 1%
Fe^{3+}	$FeOx_2$ 46%	$FeOx_3$ 25% free Fe 20% FeOx 5%	FeSu 2% $FeSu_2$ 1% $FeHPO_4$ 1%
Mg^{2+}	free Mg 87%	$MgSO_4$ 13%	
Mn^{2+}	free Mn 89%	$MnSO_4$ 10%	MnOx 1%
Ni^{2+}	free Ni 84%	$NiSO_4$ 14%	NiOx 2%
Pb^{2+}	free Pb 70%	$PbSO_4$ 25%	$PbNO_3$ 3% PbOx 2%
Sr^{2+}	free Sr 97%		$SrSO_4$ 2% $SrNO_3$ 1%
VO_2^+	free V 100%		
Zn^{2+}	free Zn 92%	$ZnSO_4$ 6% ZnOx 2%	

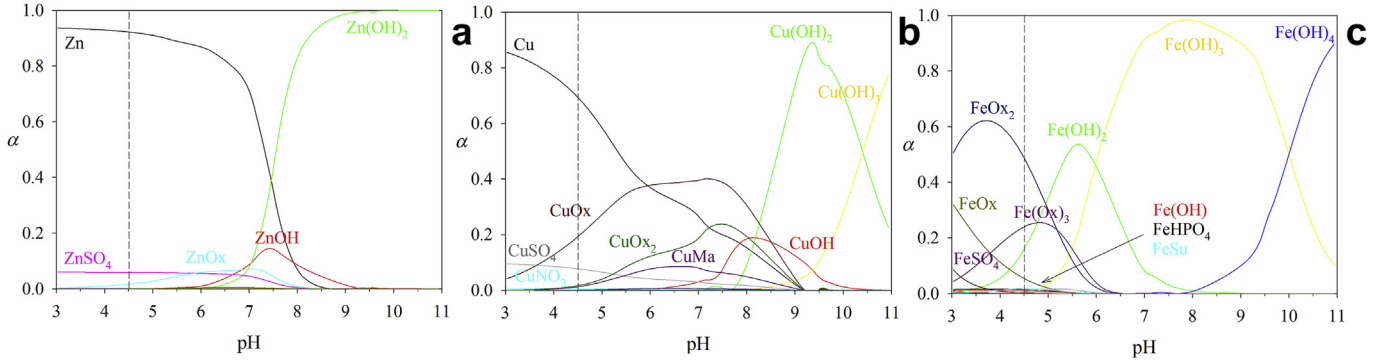

Fig. 3. Speciation diagrams obtained with reference to Zn^{2+} (*a*), Cu^{2+} (*b*), and Fe^{3+} (*c*), under the experimental conditions of this work. Speciation at pH = 4.5 are indicated as a vertical dotted line for which values are shown in Table 5.

increased the solubility of Cr by four times.

Fig. 3 shows also that at higher pH, close to neutrality, condition that may be encountered in fog droplets (Giulianelli et al., 2014) and biological fluids (Jayaraman et al., 2001), the speciation picture changes significantly. Concerning Cu (Fig. 3b), at pH close to neutrality complexation becomes increasingly important, with formation of $CuOx_2$ and CuMa complexes. Conversely for Fe (Fig. 3c), complexation becomes less important and the equilibrium shifts towards formation of non-soluble iron hydroxides.

The results obtained in this study concerning complexation of Fe^{3+} and Cu^{2+} by oxalate in simulated rain droplets are consistent with those reported by Scheinhardt et al. (2013) for aerosol samples from nine sites in Germany. Conversely, while Scheinhardt et al. (2013) found that nitrate was an important ligand for Mn^{2+}, in our study only a limited complexation of Pb^{2+} and Sr^{2+} by nitrate was found. This difference may be attributed to the different conditions considered in the two studies, i.e. deliquescent particles in Scheinhardt et al. (2013) *vs.* simulated rain droplets in the present study. Our results show that ~24% of Cu is complexed by organics, in line with the results obtained by Nimmo and Fones (1997) in rainwaters from two sites in northwest England. Conversely, we found that only ~2% of Pb and Ni were associated with organics compared with 27–28% found by Nimmo and Fones (1997) from adsorptive cathodic stripping voltammetry measurements. These contrasting results may be explained by a scarce availability of ligands, already associated with other metals, in our samples.

Availability of ligands may play a role in iron solubilisation, which was only around 6–11% on average in our samples (Table 2), lower than the 44% in coal fly ash in the presence of an excess of oxalic acid (Chen and Grassian, 2013) however higher than the 0.26% found in the more refractory Sahelian soil (Paris and Desboeufs, 2013).

Literature data (Majestic et al., 2006) suggested that Fe^{2+} may represent the most abundant fraction of soluble Fe. It may be argued that dissolved Fe^{2+} will eventually be transformed to Fe^{3+} under the typical oxidising conditions of environmental aqueous solutions, thus producing the speciation reported in Table 5 and depicted in Fig. 3. This speciation, however, represents conditions at the equilibrium, when time approaches infinity, while the oxidation of Fe^{2+} to Fe^{3+} by oxygen is relatively slow (Cotton and

Wilkinson, 1988). If Fe^{2+} is a major component of atmospheric particles, and dissolves in aqueous solution under this oxidation state, then the solution obtained will be expected to have a different speciation than that at equilibrium. The speciation calculations were thus repeated in a scenario that considers the presence of Fe^{2+} instead of Fe^{3+}, to better resemble conditions at short times after particles come into contact with water. The equilibrium constants pertaining Fe^{2+} are reported in Table 4; the results of the speciation calculation are reported in Table 6.

Fe^{3+} forms strong complexes with hard ligands such as oxalate, whereas Fe^{2+} forms only weak complexes with these organic compounds. This explains the big speciation changes which can be observed in Fe speciation at infinite and at short times (Table 5 *vs.* Table 6): Fe is mostly bound to oxalic acid if it is in the 3 + form, whereas it remains almost entirely as free ion if it is in the 2 + form. When (as in the considered aerosol sample) the total concentration of Fe is relatively large and the oxidation state is 2+, a large amount of oxalate remains available to complex other metal ions thus changing their speciation too. In particular, the fraction of oxalate complexes of Al^{3+}, Cr^{3+}, and Cu^{2+} is much larger at short times. In addition, minor changes can be observed also for some other ions, and, conversely, the fractions of free metal ions, and/or of other complexes, are generally reduced. If Fe is contained as Fe^{2+} in the PM, therefore, the solubility of all other metal ions from the PM to the aqueous solution can be further increased.

3.4. Detection of metal-ligand complexes in urban $PM_{2.5}$

Considering the concentrations and soluble fractions of the elements (Table 2) and the complexes that are most likely to form in solution (Table 5), the metal-ligand complexes that are expected to be present at the highest concentrations in our samples are those involving the metals Fe, Cu, Mn and Pb with the ligands oxalate, malonate and succinate.

In order to look for signals in the mass spectra that may be attributable to these complexes, a database was built for each possible metal-ligand combination. We considered the most stable oxidation states in aqueous solution for each element: Fe(II), Fe(III), Cu(I), Cu(II), Mn(II), Mn(III), Pb(II) and Pb(IV). Concerning the ligands, we considered both the deprotonated form and the monoprotonated form for each ligand. For the metal-ligand complex formation we considered a coordination of up to 6 with the possibility to coordinate water molecules at the sites not occupied by an organic ligand. No mixed complexes (one metal ion + two ligands, or one ligand + two metal ions) were included in the database. For each metal ion, 43 complexes were obtained and associated with their corresponding exact mass.

All possible complexes were searched for in the nanoESI-HRMS spectra as detailed in section 2.4.3; results are reported in Table 7. Of all possible combinations considered, five were found in the mass spectra of the samples. Among these, only one, an oxalate of iron (III) with formula $C_2H_3FeO_6$, was confirmed by analysis of standard solutions. Standard solutions of iron(III) oxalates ($[Fe^{3+}] = 2.32 \cdot 10^{-5}$ M; $[Ox^{2-}] = 2.20 \cdot 10^{-4}$ M) in water/methanol (50:50) at pH 2.6, 3.2 and 4.0 and in methanol at autogenic pH presented peaks in the mass spectra of the oxalate anion, and the oxalate of iron(III) with stoichiometry 2:1 (with neutral formula C_4HFeO_8). In the solution at pH 4, more similar to sample conditions, the oxalate of iron(III) with stoichiometry 1:1 (with neutral formula $C_2H_3FeO_6$) was also detected, thus confirming the signal that was assigned in the real samples (species in bold in Table 7). However, the ratio between C_4HFeO_8 and $C_2H_3FeO_6$ is about 10:1 in the standard solution while $C_2H_3FeO_6$ is the only detected species in the real samples. This discrepancy between real samples and standard solutions may be due to different oxalate concentrations in the real samples and/or matrix effects that might have influenced fragmentation in the ESI source. Further work is needed to confirm the presence of metal-ligand complexes in atmospheric aerosol, including measurements without prior extraction in an aqueous or organic solvent that may introduce artefacts.

The samples in which the iron oxalate complex was detected were collected on the 3rd January 2014 and on the 8th January 2014. These two days were characterised by a relatively high aerosol concentration ($PM_{2.5}$ 74 μg m^{-3} on the 8th January) and ambient temperature was close to the dewpoint temperature (Lawrence, 2005) therefore indicating a high probability of fog formation favouring aqueous phase chemistry. These were the only two days in which both conditions (high aerosol loading and high probability of fog formation) occurred simultaneously.

Table 6
Percentages of the various metal ions species calculated on the basis of the thermodynamic model of Table 4, under the hypothesis that all Fe was Fe(II) rather than Fe(III), for the PM sampled on 10th January 2014 (concentrations in the extraction solution at pH 4.5, simulating rain droplet composition). Only species having percentages above 1% are reported. Free metal ion percentages (given as sum of percentages of M^{n+} and of its hydroxo derivatives) are reported also if below 1%. Values in bold indicate a marked difference between percentages reported here and those reported in Table 5.

metal ion	major species	other important species (>5%)	minor species (<5%)
Al^{3+}	**$Al(Ox)_2$ 63%**	$Al(Ox)_3$ 35%	**AlOx 2%** AlMa <1% free Al < 1%
Ca^{2+}	free Ca 91%	$CaSO_4$ 8%	$CaNO_3$ 1%
Cd^{2+}	free Cd 86%	$CdSO_4$ 12%	CdCl 1% $CdNO_3$ 1%
Co^{2+}	free Co 81%	$CoSO_4$ 16%	CoOx 3%
Cr^{3+}	**$CrOx_3$ 47%**	**$CrOx_2$ 27%** CrOx 9% **CrSu 6% free Cr 6%**	**CrMa 4%** $CrSu_2$ < 1% $CrMa_2$ < 1%
Cu^{2+}	**free Cu 47%**	**CuOx 37%** **$CuOx_2$ 10%** $CuSO_4$ 5%	CuMa 1%
Fe^{2+}	**free Fe 87%**	**$FeSO_4$ 13%**	**FeOx complexes < 1%**
Mg^{2+}	free Mg 87%	$MgSO_4$ 13%	
Mn^{2+}	free Mn 88%	$MnSO_4$ 9%	MnOx 3%
Ni^{2+}	free Ni 81%	$NiSO_4$ 14% NiOx 5%	
Pb^{2+}	free Pb 68%	$PbSO_4$ 24% PbOx 5%	$PbNO_3$ 3%
Sr^{2+}	free Sr 97%		$SrSO_4$ 2% $SrNO_3$ 1%
VO_2^+	free V 100%		
Zn^{2+}	free Zn 89%	$ZnSO_4$ 6% ZnOx 5%	

4. Conclusions

We investigated the formation of metal-ligand complexes, and how this process may affect the solubility of metals, in urban atmospheric aerosol samples collected in the city centre of Padua (Italy) from the 5th December 2013 to the 1st April 2014. Short-chain dicarboxylic acids, i.e. oxalate, succinate, and malonate, were abundant aerosol components in the collected samples that possess ligand properties. We found that organic ligand concentrations are significantly correlated with the soluble fraction of non-readily soluble metals, such as Fe.

PCA applied to the soluble fractions of all metals and the concentration of both organic and inorganic anions showed that very soluble metals, such as Zn, K, Rb, and Mg, are not associated with the presence of the organic ligands. Fe and Pb, on the contrary, are the elements whose solubility is strongly associated with the presence of the organic ligands. A speciation analysis in solution at pH 4.5, simulating fog/rainwater, pointed out that many metals are

Table 7
Detected metal-ligand (ML) complexes in nanoESI-HRMS spectra (in negative ionisation mode) of $PM_{2.5}$ samples collected from the 5th December 2013 to the 1st April 2014. The species in bold was confirmed by analysis of standard solutions.

Formula	Metal ion	Ligands	Coordinating water molecules	Adducts	Detected ion	Samples in which ML were detected
$C_8H_{16}FeO_{11}$	Fe^{2+}	2 x ($Su^{2-} + H^+$)	3 x (H_2O)	Cl^-, For^-	$[ML + Cl + For]^{2-}$	QF11-W
$C_2H_3FeO_6$	**Fe^{3+}**	**Ox^{2-}**	**$H_2O + OH^-$**	**Cl^-**	**$[ML + Cl]^-$**	**QF8-W, QF9-W**
$C_{16}H_{23}MnO_{17}$	Mn^{3+}	4 x ($Su^{2-} + H^+$)	H_2O	For^-, Ac^-	$[ML + For + Ac]^{3-}$	QF6-W, QF16-W
$C_6H_7CuO_9Na$	Cu^{2+}	2 x Ma^{2-}	H_2O	Na^+	$[ML + Na]^-$	QF1-W, QF9-W, QF10-W
$C_{16}H_{27}CuO_{17}N$	Cu^{2+}	4 x ($Su^{2-} + H^+$)	H_2O	NH_4^+, For^-	$[ML + NH_4 + For]^-$	QF15-W, QF17-W, QF18-W

either partly complexed with oxalate, malonate and succinate, like Cu, Zn, Mn, Pb, and Ni, or completely complexed with the same diacids, like Al, Cr and Fe. The solubility increments of Al and Fe due to aerosol components can be estimated to be around two orders of magnitudes, while for Cr the solubility is increased by four times due to the presence of diacids. According to our results, the oxidation state of Fe can have a significant effect on the speciation of this and of other metal ions dissolving in aqueous solution. Further studies appear necessary to obtain information on the oxidation state of Fe, both when contained in PM and once released in an aqueous solution, to allow an accurate prediction of the speciation picture of PM components.

Direct analysis of aerosol extracts in methanol with nanoESI-HRMS showed the presence of a signal of a 1:1 complex between Fe(III) and oxalate in two samples collected on days characterised by high aerosol loading and high probability of fog formation, indicating that these complexes can be identified directly.

The study here reported considers metal speciation at equilibrium and confirms, using both quantitative data and a thermodynamic model, that important environmental and health properties of the aerosol may be influenced by metal-ligand interactions in the specific media. The solubility changes of metal ions potentially induced by complexation with organics affect the bioaccessibility (Wiseman, 2015) of the metals themselves. Formation of complexes can also impact redox chemistry, therefore the ability of metals to deplete antioxidants in the lungs once particles are inhaled and come into contact with lung fluids. Further work is needed to investigate the kinetic of solubilisation of the metals and how it is affected by other aerosol components.

Acknowledgements

This work was partly funded by the Supporting TAlent in ReSearch@ University of Padova STARS-StG MOCAA to CG and by the European Research Council ERC consolidator grant 279405 to MK.

Appendix A. Supplementary data

Supplementary data to this article can be found online at https://doi.org/10.1016/j.chemosphere.2019.125025.

References

Badocco, D., Lavagnini, I., Mondin, A., Pastore, P., 2014. Estimation of the uncertainty of the quantification limit. Spectrochim. Acta Part B At. Spectrosc. 96, 8–11. https://doi.org/10.1016/j.sab.2014.03.013.

Badocco, D., Lavagnini, I., Mondin, A., Pastore, P., 2015a. Effect of multiple error sources on the calibration uncertainty. Food Chem. 177, 147–151. https://doi.org/10.1016/j.foodchem.2015.01.020.

Badocco, D., Lavagnini, I., Mondin, A., Tapparo, A., Pastore, P., 2015b. Limit of detection in the presence of instrumental and non-instrumental errors : study of the possible sources of error and application to the analysis of 41 elements at trace levels by inductively coupled plasma-mass spectrometry technique. Spectrochim. Acta Part B At. Spectrosc. 107, 178–184. https://doi.org/10.1016/j.sab.2015.03.009.

Beiderwieden, E., Wrzesinsky, T., Klemm, O., 2005. Chemical characterization of fog and rain water collected at the eastern Andes cordillera. Hydrol. Earth Syst. Sci. Discuss. 2 (3), 863–885. https://doi.org/10.5194/hessd-2-863-2005.

Birmili, W., Allen, A.G., Bary, F., Harrison, R.M., 2006. Trace metal concentrations and water solubility in size-fractionated atmospheric particles and influence of road traffic. Environ. Sci. Technol. 40 (4), 1144–1153. https://doi.org/10.1021/es0486925.

Borgatta, J., Navea, J.G., 2015. Fate of aqueous iron leached from tropospheric aerosols during atmospheric acidic processing: a study of the effect of humic-like substances. WIT Trans. Ecol. Environ. 198 (Iii), 155–166. https://doi.org/10.2495/AIR150131.

Burnett, R., Chen, H., Szyszkowicz, M., Fann, N., Hubbell, B., Pope, C.A., Apte, J.S., Brauer, M., Cohen, A., Weichenthal, S., Coggins, J., Di, Q., Brunekreef, B., Frostad, J., Lim, S.S., Kan, H., Walker, K.D., Thurston, G.D., Hayes, R.B., Lim, C.C., Turner, M.C., Jerrett, M., Krewski, D., Gapstur, S.M., Diver, W.R., Ostro, B., Goldberg, D., Crouse, D.L., Martin, R.V., Peters, P., Pinault, L., Tjepkema, M., van Donkelaar, A., Villeneuve, P.J., Miller, A.B., Yin, P., Zhou, M., Wang, L., Janssen, N.A.H., Marra, M., Atkinson, R.W., Tsang, H., Quoc Thach, T., Cannon, J.B., Allen, R.T., Hart, J.E., Laden, F., Cesaroni, G., Forastiere, F., Weinmayr, G., Jaensch, A., Nagel, G., Concin, H., Spadaro, J.V., 2018. Global estimates of mortality associated with long-term exposure to outdoor fine particulate matter. Proc. Natl. Acad. Sci. 115 (38), 9592–9597. https://doi.org/10.1073/pnas.1803222115.

Cheize, M., Sarthou, G., Croot, P.L., Bucciarelli, E., Baudoux, A.C., Baker, A.R., 2012. Iron organic speciation determination in rainwater using cathodic stripping voltammetry. Anal. Chim. Acta 736, 45–54. https://doi.org/10.1016/j.aca.2012.05.011.

Chen, H., Grassian, V.H., 2013. Iron dissolution of dust source materials during simulated acidic processing: the effect of sulfuric, acetic, and oxalic acids. Environ. Sci. Technol. 47 (18), 10312–10321. https://doi.org/10.1021/es401285s.

Chen, L.C., Lippmann, M., 2009. Effects of metals within ambient air particulate matter (PM) on human health. Inhal. Toxicol. 21 (1), 1–31. https://doi.org/10.1080/08958370802105405 [online] Available from: http://www.tandfonline.com/doi/abs/10.1080/08958370802105405?journalCode=iiht20. (Accessed 19 November 2015).

Chianese, E., Tirimberio, G., Riccio, A., 2019. PM2.5 and PM10 in the urban area of Naples: chemical composition, chemical properties and influence of air masses origin. J. Atmos. Chem. 76 (2), 151–169. https://doi.org/10.1007/s10874-019-09392-3.

Cotton, F.A., Wilkinson, G., 1988. Advanced Inorganic Chemistry, fifth ed. John Wiley and Sons, Inc.

Csavina, J., Field, J., Taylor, M.P., Gao, S., Landázuri, A., Betterton, E.A., Sáez, A.E., 2012. A review on the importance of metals and metalloids in atmospheric dust and aerosol from mining operations. Sci. Total Environ. 433, 58–73. https://doi.org/10.1016/j.scitotenv.2012.06.013.

Decesari, S., Sowlat, M.H., Hasheminassab, S., Sandrini, S., Gilardoni, S., Facchini, M.C., Fuzzi, S., Sioutas, C., 2017. Enhanced toxicity of aerosol in fog conditions in the Po Valley, Italy. Atmos. Chem. Phys. Discuss. (February), 1–19. https://doi.org/10.5194/acp-2017-118.

Deguillaume, L., Leriche, M., Desboeufs, K., Mailhot, G., George, C., Chaumerliac, N., 2005. Transition metals in atmospheric liquid phases: sources, reactivity, and sensitive parameters. Chem. Rev. 105, 3388–3431. https://doi.org/10.1021/cr040649c.

DePalma, S.G.S., Arnold, W.R., McGeer, J.C., Dixon, D.G., Smith, D.S., 2011. Effects of dissolved organic matter and reduced sulphur on copper bioavailability in coastal marine environments. Ecotoxicol. Environ. Saf. 74 (3), 230–237. https://doi.org/10.1016/j.ecoenv.2010.12.003.

Elzinga, E.J., Gao, Y., Fitts, J.P., Tappero, R., 2011. Iron speciation in urban dust. Atmos. Environ. 45 (26), 4528–4532. https://doi.org/10.1016/j.atmosenv.2011.05.042.

Fomba, K.W., Van Pinxteren, D., Müller, K., Iinuma, Y., Lee, T., Collett, J.L., Herrmann, H., 2015. Trace metal characterization of aerosol particles and cloud water during HCCT 2010. Atmos. Chem. Phys. 15 (15), 8751–8765. https://doi.org/10.5194/acp-15-8751-2015.

Franzetti, A., Gandolfi, I., Gaspari, E., Ambrosini, R., Bestetti, G., 2011. Seasonal variability of bacteria in fine and coarse urban air particulate matter. Appl. Microbiol. Biotechnol. 90 (2), 745–753. https://doi.org/10.1007/s00253-010-3048-7.

Freitas, A. de M., Martins, L.D., Solci, M.C., 2012. Size-segregated particulate matter and carboxylic acids over urban and rural sites in Londrina City, Brazil. J. Braz. Chem. Soc. 23 (5), 921–930. https://doi.org/10.1590/S0103-50532012000500018.

Giorio, C., Tapparo, A., Scapellato, M.L., Carrieri, M., Apostoli, P., Bartolucci, G.B.,

2013. Field comparison of a personal cascade impactor sampler, an optical particle counter and CEN-EU standard methods for PM10, PM2.5 and PM1 measurement in urban environment. J. Aerosol Sci. 65, 111–120. https://doi.org/10.1016/j.jaerosci.2013.07.013.

Giorio, C., Moyroud, E., Glover, B.J., Skelton, P.C., Kalberer, M., 2015. Direct surface analysis coupled to high-resolution mass spectrometry reveals heterogeneous composition of the cuticle of Hibiscus trionum petals. Anal. Chem. 87 (19), 9900–9907. https://doi.org/10.1021/acs.analchem.5b02498.

Giorio, C., Marton, D., Formenton, G., Tapparo, A., 2017. formation of metal–cyanide complexes in deliquescent airborne particles: a new possible sink for HCN in urban environments. Environ. Sci. Technol. 51 (24), 14107–14113. https://doi.org/10.1021/acs.est.7b03123.

Giorio, C., Bortolini, C., Kourtchev, I., Tapparo, A., Bogialli, S., Kalberer, M., 2019a. Direct target and non-target analysis of urban aerosol sample extracts using atmospheric pressure photoionisation high-resolution mass spectrometry. Chemosphere 224, 786–795. https://doi.org/10.1016/j.chemosphere.2019.02.151.

Giorio, C., Pizzini, S., Marchiori, E., Piazza, R., Grigolato, S., Zanetti, M., Cavalli, R., Simoncin, M., Soldà, L., Badocco, D., Tapparo, A., 2019b. Sustainability of using vineyard pruning residues as an energy source: combustion performances and environmental impact. Fuel 243, 371–380. https://doi.org/10.1016/j.fuel.2019.01.128.

Giulianelli, L., Gilardoni, S., Tarozzi, L., Rinaldi, M., Decesari, S., Carbone, C., Facchini, M.C., Fuzzi, S., 2014. Fog occurrence and chemical composition in the Po valley over the last twenty years. Atmos. Environ. 98, 394–401. https://doi.org/10.1016/j.atmosenv.2014.08.080.

Grosjean, D., 1992. Formic acid and acetic acid: emissions, atmospheric formation and dry deposition at two southern California locations. Atmos. Environ. Part A, Gen. Top. 26 (18), 3279–3286. https://doi.org/10.1016/0960-1686(92)90343-J.

Harrison, R.M., Giorio, C., Beddows, D.C.S., Dall'Osto, M., 2010. Size distribution of airborne particles controls outcome of epidemiological studies. Sci. Total Environ. 409 (2), 289–293. https://doi.org/10.1016/j.scitotenv.2010.09.043.

Jayaraman, S., Song, Y., Vetrivel, L., Shankar, L., Verkman, A.S., 2001. Noninvasive in vivo fluorescence measurement of airway-surface liquid depth, salt concentration, and pH. J. Clin. Investig. 107 (3), 317–324. https://doi.org/10.1172/JCI11154.

Jickells, T.D., An, Z.S., Andersen, K.K., Baker, A.R., Bergametti, G., Brooks, N., Cao, J.J., Boyd, P.W., Duce, R.A., Hunter, K.A., Kawahata, H., Kubilay, N., laRoche, J., Liss, P.S., Mahowald, N., Prospero, J.M., Ridgwell, A.J., Tegen, I., Torres, R., 2005. Global iron connections between desert dust, ocean biogeochemistry, and climate. Science 308 (5718), 67–71. https://doi.org/10.1126/science.1105959.

Kawamura, K., Bikkina, S., 2016. A review of dicarboxylic acids and related compounds in atmospheric aerosols: molecular distributions, sources and transformation. Atmos. Res. 170, 140–160. https://doi.org/10.1016/j.atmosres.2015.11.018.

Kerminen, V.-M., Ojanen, C., Pakkanen, T., Hillamo, R., Aurela, M., Meriläinen, J., 2000. Low-molecular-WEIGHT dicarboxylic acids IN an urban and rural atmosphere. J. Aerosol Sci. 31 (3), 349–362. https://doi.org/10.1016/S0021-8502(99)00063-4.

Kourtchev, I., O'Connor, I.P., Giorio, C., Fuller, S.J., Kristensen, K., Maenhaut, W., Wenger, J.C., Sodeau, J.R., Glasius, M., Kalberer, M., 2014. Effects of anthropogenic emissions on the molecular composition of urban organic aerosols: an ultrahigh resolution mass spectrometry study. Atmos. Environ. 89, 525–532. https://doi.org/10.1016/j.atmosenv.2014.02.051.

Lawrence, M.G., 2005. The relationship between relative humidity and the dewpoint temperature in moist air: a simple conversion and applications. Bull. Am. Meteorol. Soc. 86 (2), 225–233. https://doi.org/10.1175/BAMS-86-2-225.

Lelieveld, J., Evans, J.S., Fnais, M., Giannadaki, D., Pozzer, A., 2015. The contribution of outdoor air pollution sources to premature mortality on a global scale. Nature 525 (7569), 367–371. https://doi.org/10.1038/nature15371.

Lelieveld, J., Klingmüller, K., Pozzer, A., Pöschl, U., Fnais, M., Daiber, A., Münzel, T., 2019. Cardiovascular disease burden from ambient air pollution in Europe reassessed using novel hazard ratio functions. Eur. Heart J. 1–7. https://doi.org/10.1093/eurheartj/ehz135.

Li, Y.C., Yu, J.Z., 2005. Simultaneous determination of mono- and dicarboxylic acids, ω-oxo-carboxylic acids, midchain ketocarboxylic acids, and aldehydes in atmospheric aerosol samples. Environ. Sci. Technol. 39 (19), 7616–7624. https://doi.org/10.1021/es050896d.

Liu, J., Zhang, X., Parker, E.T., Veres, P.R., Roberts, J.M., de Gouw, J.A., Hayes, P.L., Jimenez, J.L., Murphy, J.G., Ellis, R.A., Huey, L.G., Weber, R.J., 2012. On the gas-particle partitioning of soluble organic aerosol in two urban atmospheres with contrasting emissions: 2. Gas and particle phase formic acid. J. Geophys. Res. Atmos. 117 (D21) https://doi.org/10.1029/2012JD017912 n/a-n/a.

Majestic, B.J., Schauer, J.J., Shafer, M.M., Turner, J.R., Fine, P.M., Singh, M., Sioutas, C., 2006. Development of a wet-chemical method for the speciation of iron in atmospheric aerosols. Environ. Sci. Technol. 40 (7), 2346–2351. https://doi.org/10.1021/es052023p.

Di Marco, V.B., 1998. Studio della formazione di complessi tra alluminio e molecole di interesse ambientale, biologico e farmaceutico, 11 November. Available from: http://paduaresearch.cab.unipd.it/7349/. (Accessed 25 May 2019).

Mkoma, S.L., da Rocha, G.O., da Silva, J.D.S., de Andrade, J.B., 2012. Characteristics of low-molecular weight carboxylic acids in PM2.5 and PM10 ambient aerosols from Tanzania. In: Atmospheric Aerosols - Regional Characteristics - Chemistry and Physics. InTech., pp. 203–219

Mooibroek, D., Schaap, M., Weijers, E.P., Hoogerbrugge, R., 2011. Source apportionment and spatial variability of PM 2.5 using measurements at five sites in The Netherlands. Atmos. Environ. 45 (25), 4180–4191. https://doi.org/10.1016/j.atmosenv.2011.05.017.

Nieberding, F., Breuer, B., Braeckevelt, E., Klemm, O., Song, Q., Zhang, Y., 2018. Fog water chemical composition on ailaoshan mountain, Yunnan province, SW China. Aerosol Air Qual. Res. 18 (1), 37–48. https://doi.org/10.4209/aaqr.2017.01.0060.

Nimmo, M., Fones, G.R., 1997. The potential pool of Co, Ni, Cu, Pb and Cd organic complexing ligands in coastal and urban rain waters. Atmos. Environ. 31 (5), 693–702. https://doi.org/10.1016/S1352-2310(96)00243-9.

Oberdörster, G., Oberdörster, E., Oberdörster, J., 2005. Nanotoxicology: an emerging discipline evolving from studies of ultrafine particles. Environ. Health Perspect. 113 (7), 823–839. https://doi.org/10.1289/ehp.7339.

Okochi, H., Brimblecombe, P., 2002. Potential trace metal-organic complexation in the atmosphere. ScientificWorldJournal 2, 767–786. https://doi.org/10.1100/tsw.2002.132.

Pant, P., Shi, Z., Pope, F.D., Harrison, R.M., 2017. Characterization of traffic-related particulate matter emissions in a road tunnel in Birmingham, UK: trace metals and organic molecular markers. Aerosol Air Qual. Res. 17 (1), 117–130. https://doi.org/10.4209/aaqr.2016.01.0040.

Paris, R., Desboeufs, K.V., 2013. Effect of atmospheric organic complexation on iron-bearing dust solubility. Atmos. Chem. Phys. 13 (9), 4895–4905. https://doi.org/10.5194/acp-13-4895-2013.

Paris, R., Desboeufs, K.V., Journet, E., 2011. Variability of dust iron solubility in atmospheric waters: investigation of the role of oxalate organic complexation. Atmos. Environ. 45 (36), 6510–6517. https://doi.org/10.1016/j.atmosenv.2011.08.068.

Perrone, M.G., Gualtieri, M., Ferrero, L., Porto, C. Lo, Udisti, R., Bolzacchini, E., Camatini, M., 2010. Seasonal variations in chemical composition and in vitro biological effects of fine PM from Milan. Chemosphere. https://doi.org/10.1016/j.chemosphere.2009.12.071.

Perrone, M.G., Larsen, B.R., Ferrero, L., Sangiorgi, G., De Gennaro, G., Udisti, R., Zangrando, R., Gambaro, A., Bolzacchini, E., 2012. Sources of high PM2.5 concentrations in Milan, Northern Italy: molecular marker data and CMB modelling. Sci. Total Environ. 414, 343–355. https://doi.org/10.1016/j.scitotenv.2011.11.026.

Pietrogrande, M.C., Bacco, D., Visentin, M., Ferrari, S., Poluzzi, V., 2014. Polar organic marker compounds in atmospheric aerosol in the Po Valley during the Supersito campaigns — Part 1: low molecular weight carboxylic acids in cold seasons. Atmos. Environ. 86, 164–175. https://doi.org/10.1016/j.atmosenv.2013.12.022.

Press, W.H., Teukolsky, S.A., Vetterling, W.T., Flannery, B.P., 2007. Cambridge University Press: numerical recipes : the art of scientific computing [online] Available from: https://www.cambridge.org/it/academic/subjects/mathematics/numerical-recipes/numerical-recipes-art-scientific-computing-3rd-edition?format=HB&utm_source=shortlink&utm_medium=shortlink&utm_campaign=numericalrecipes. (Accessed 25 May 2019).

Querol, X., Alastuey, A., Moreno, T., Viana, M.M., Castillo, S., Pey, J., Rodríguez, S., Artiñano, B., Salvador, P., Sánchez, M., Garcia Dos Santos, S., Herce Garraleta, M.D., Fernandez-Patier, R., Moreno-Grau, S., Negral, L., Minguillón, M.C., Monfort, E., Sanz, M.J., Palomo-Marín, R., Pinilla-Gil, E., Cuevas, E., de la Rosa, J., Sánchez de la Campa, A., 2008. Spatial and temporal variations in airborne particulate matter (PM 10 and PM 2.5) across Spain 1999-2005. Atmos. Environ. 42 (17), 3964–3979. https://doi.org/10.1016/j.atmosenv.2006.10.071.

Raaschou-Nielsen, O., Andersen, Z.J., Beelen, R., Samoli, E., Stafoggia, M., Weinmayr, G., Hoffmann, B., Fischer, P., Nieuwenhuijsen, M.J., Brunekreef, B., Xun, W.W., Katsouyanni, K., Dimakopoulou, K., Sommar, J., Forsberg, B., Modig, L., Oudin, A., Oftedal, B., Schwarze, P.E., Nafstad, P., De Faire, U., Pedersen, N.L., Östenson, C.-G., Fratiglioni, L., Penell, J., Korek, M., Pershagen, G., Eriksen, K.T., Sørensen, M., Tjønneland, A., Ellermann, T., Eeftens, M., Peeters, P.H., Meliefste, K., Wang, M., Bueno-de-Mesquita, B., Key, T.J., de Hoogh, K., Concin, H., Nagel, G., Vilier, A., Grioni, S., Krogh, V., Tsai, M.-Y., Ricceri, F., Sacerdote, C., Galassi, C., Migliore, E., Ranzi, A., Cesaroni, G., Badaloni, C., Forastiere, F., Tamayo, I., Amiano, P., Dorronsoro, M., Trichopoulou, A., Bamia, C., Vineis, P., Hoek, G., 2013. Air pollution and lung cancer incidence in 17 European cohorts: prospective analyses from the European study of cohorts for air pollution effects (ESCAPE). Lancet Oncol. 14 (9), 813–822. https://doi.org/10.1016/S1470-2045(13)70279-1.

Rodhe, H., Dentener, F., Schulz, M., 2002. The global distribution of acidifying wet deposition. Environ. Sci. Technol. 36 (20), 4382–4388. https://doi.org/10.1021/es020057g.

Rogula-Kozłowska, W., Klejnowski, K., Rogula-Kopiec, P., Ośródka, L., Krajny, E., Błaszczak, B., Mathews, B., 2014. Spatial and seasonal variability of the mass concentration and chemical composition of PM 2.5 in Poland. Air Qual. Atmos. Heal. 7 (1), 41–58. https://doi.org/10.1007/s11869-013-0222-y.

Sareen, N., Carlton, A.G., Surratt, J.D., Gold, A., Lee, B., Lopez-Hilfiker, F.D., Mohr, C., Thornton, J.A., Zhang, Z., Lim, Y.B., Turpin, B.J., 2016. Identifying precursors and aqueous organic aerosol formation pathways during the SOAS campaign. Atmos. Chem. Phys. 16 (22), 14409–14420. https://doi.org/10.5194/acp-16-14409-2016.

Scheinhardt, S., Müller, K., Spindler, G., Herrmann, H., 2013. Complexation of trace metals in size-segregated aerosol particles at nine sites in Germany. Atmos. Environ. 74, 102–109. https://doi.org/10.1016/j.atmosenv.2013.03.023.

Schroth, A.W., Crusius, J., Sholkovitz, E.R., Bostick, B.C., 2009. Iron solubility driven

by speciation in dust sources to the ocean. Nat. Geosci. 2 (5), 337–340. https://doi.org/10.1038/ngeo501.
ScQuery v.5.84, 2005. the Iupac Stability Constant Database. Academic Software, Copyright.
Shiraiwa, M., Ueda, K., Pozzer, A., Lammel, G., Kampf, C.J., Fushimi, A., Enami, S., Arangio, A.M., Fröhlich-Nowoisky, J., Fujitani, Y., Furuyama, A., Lakey, P.S.J., Lelieveld, J., Lucas, K., Morino, Y., Pöschl, U., Takahama, S., Takami, A., Tong, H., Weber, B., Yoshino, A., Sato, K., 2017. Aerosol health effects from molecular to global scales. Environ. Sci. Technol. 51 (23), 13545–13567. https://doi.org/10.1021/acs.est.7b04417.
Tong, H.-J., Fitzgerald, C., Gallimore, P.J., Kalberer, M., Kuimova, M.K., Seville, P.C., Ward, A.D., Pope, F.D., 2014. Rapid interrogation of the physical and chemical characteristics of salbutamol sulphate aerosol from a pressurised metered-dose inhaler (pMDI). Chem. Commun. 50 (3), 3–6. https://doi.org/10.1039/c4cc05803h.
Topinka, J., Rossner, P., Milcova, A., Schmuczerova, J., Svecova, V., Sram, R.J., 2011. DNA adducts and oxidative DNA damage induced by organic extracts from PM2.5 in an acellular assay. Toxicol. Lett. 202 (3), 186–192. https://doi.org/10.1016/J.TOXLET.2011.02.005.
Vinatier, V., Wirgot, N., Joly, M., Sancelme, M., Abrantes, M., Deguillaume, L., Delort, A.M., 2016. Siderophores in cloud waters and potential impact on atmospheric chemistry: production by microorganisms isolated at the puy de Dôme station. Environ. Sci. Technol. 50 (17), 9315–9323. https://doi.org/10.1021/acs.est.6b02335.
Walna, B., 2015. Results of long−term observations of basic physico−chemical data of atmospheric precipitation in a protected area in Western Poland, Atmos. Pollut. Res. 6 (4), 651–661. https://doi.org/10.5094/apr.2015.074.
Wang, P., Bi, S.P., Zhou, Y.P., Tao, Q.S., Gan, W.X., Xu, Y., Hong, Z., Cai, W.S., 2007. Study of aluminium distribution and speciation in atmospheric particles of different diameters in Nanjing, China, Atmos. Environ. Times 41 (27), 5788–5796. https://doi.org/10.1016/j.atmosenv.2007.01.064.
Wang, Y., Yu, W., Pan, Y., Wu, D., 2012. Acid neutralization of precipitation in Northern China. J. Air Waste Manag. Assoc. 62 (2), 204–211. https://doi.org/10.1080/10473289.2011.640761.
Wei, J., Yu, H., Wang, Y., Verma, V., 2019. Complexation of iron and copper in ambient particulate matter and its effect on the oxidative potential measured in a surrogate lung fluid. Environ. Sci. Technol. 53 (3), 1661–1671. https://doi.org/10.1021/acs.est.8b05731.
WHO, W.H.O., 2016. Ambient Air Pollution: a global assessment of exposure and burden of disease. World Health Organ. doi:9789241511353.
Willey, J.D., Kieber, R.J., Williams, K.H., Crozier, J.S., Skrabal, S.A., Avery, G.B., 2000. Temporal variability of iron speciation in coastal rainwater. J. Atmos. Chem. 37 (2), 185–205. https://doi.org/10.1023/A:1006421624865.
Win, M.S., Tian, Z., Zhao, H., Xiao, K., Peng, J., Shang, Y., Wu, M., Xiu, G., Lu, S., Yonemochi, S., Wang, Q., 2018. Atmospheric HULIS and its ability to mediate the reactive oxygen species (ROS): a review. J. Environ. Sci. (China) 71, 13–31. https://doi.org/10.1016/j.jes.2017.12.004.
Wiseman, C.L.S., 2015. Analytical methods for assessing metal bioaccessibility in airborne particulate matter: a scoping review. Anal. Chim. Acta 877, 9–18. https://doi.org/10.1016/j.aca.2015.01.024.
Yao, X., Fang, M., Chan, C.K., Ho, K.F., Lee, S.C., 2004. Characterization of dicarboxylic acids in PM2.5 in Hong Kong. Atmos. Environ. 38 (7), 963–970. https://doi.org/10.1016/j.atmosenv.2003.10.048.
Zhang, R., Wang, G., Guo, S., Zamora, M.L., Ying, Q., Lin, Y., Wang, W., Hu, M., Wang, Y., 2015. formation of urban fine particulate matter. Chem. Rev. 115 (10), 3803–3855. https://doi.org/10.1021/acs.chemrev.5b00067.